

Biodegradable Materials for Multilayer Transient Printed Circuit Boards

Xian Huang, Yuhao Liu, Suk-Won Hwang, Seung-Kyun Kang, Dwipayan Patnaik, Jonathan Fajardo Cortes, and John A. Rogers*

Printed circuit boards (PCBs) are essential components of nearly all forms of commercial electronics, where they provide mechanical supports and electrical interconnections for mounted components. Modern PCBs offer multilayer configurations, capable of high frequency signal conduction with minimal transmission loss, and robust, reliable performance in various environmental conditions over extended periods of time. The constituent materials typically include metals such as gold, silver, palladium, tin, and copper, on substrates and interlayer dielectrics of fiber glass or polyimide, for rigid^[1] or flexible [2] PCBs, respectively. These materials are designed explicitly for chemical stability and negligible degradation under long-term use.

Increasing demands for the latest consumer electronics technologies together with an accelerated rate of obsolescence generates expanding volumes of electronic waste (25×10^6 ton/year),^[2] the majority (82%) of which appears in landfills,^[3] where the circuits are slow to degrade due to designs that are optimized for robustness and survivability. Release of toxic materials such as lead, mercury, cadmium, polyvinyl chloride, and brominated flame retardants can pollute ground water and soil,^[4,5] with environmental effects that can adversely affect both physiological and psychological wellness.^[6–8] Recovering metals and plastics from PCBs involves chemical separation,^[9] burning,^[10] and mechanical shredding^[11] processes, each of which involves occupational and environmental hazards.^[12–14]

One potential route to reduce electronic waste streams is to build the electronics using materials that can naturally degrade into biologically and environmentally benign end products on timescales that exceed desired device lifetimes.^[15] Recently developed classes of 'transient' electronic components, such as transistors,^[16] mechanical energy harvesters,^[17] electrodes,^[15] and primary batteries^[18] as well as functional circuits for radio transmission and power harvesting^[19] offer these characteristics

in systems that involve water soluble active and passive materials. Transient PCBs have not, however, been demonstrated. The work reported here addresses this unmet need through the introduction of materials and fabrication procedures for biodegradable PCBs. Several application examples demonstrate the utility of these platforms.

Figure 1a shows the structure of a transient PCB (23 mm × 23 mm) that consists of stacked layers of transient metal traces and dielectric interlayers on a flexible support. This device example harvests radio frequency (RF) energy, senses the ambient temperature and transmits the corresponding data via a wireless signal. The construction involves two separately fabricated sodium carboxymethylcellulose (Na-CMC) substrates (~50 μm in thickness) with electrical interconnects made of transient metals (2 μm in thickness), e.g., magnesium (Mg), tungsten (W), and/or zinc (Zn).^[20] A layer of poly(ethylene oxide) (PEO) (1 μm in thickness) between the Na-CMC films bonds them together (Figure 1a and 1b). Transient metal pastes (Figure S1a) enable mounting of commercial-of-the-shelf (COTS) components onto contact pads located on these platforms. The pastes consist of either W or Zn microparticles (4 to 12 μm in average diameter) dispersed in a binder of PEO in an organic solvent. Evaporation of the solvent at room temperature yields a solidified metal/polymer composite that offers good conductivity (up to 40 kS/m) and also serves as an adhesive between the pins of the COTS components and the PCB (Figure 1c). The solidified paste has good mechanical strength, with the ability to retain COTS components bonded to the circuit pads even under repeated bending. The primary failure mode, in fact, is delamination of the pads from the substrate, rather than cohesive failure of the pastes or adhesive failure at their interfaces. Filling via holes with a W paste electrically connects the bottom and top circuit patterns (Figure 1d), thereby allowing signal communication and power transmission. This set of materials forms a flexible laminate (Figure 1e) capable of serving as a foundation for complex circuit assembly.

The system of Figure 1 measures variations in ambient temperature and communicates the results to an external recording system through a frequency-modulated wireless signal. Testing involves placing the system on the outer side of a window, with a receiving antenna located indoors (Figure S2a). A transmission antenna, also indoors and located 30 cm away from the circuit provides power that allows the generation of a voltage (3V) by the wireless power harvester for operating the entire circuit (Figure S2b and S2d). The frequency of the wireless signal transmitted by the circuit increases from 2.47 to 2.49 GHz as the temperature varies from 35 to 18 °C. The amplitude of the

Dr. X. Huang, Y. Liu, Dr. S.-W. Hwang, Dr. S.-K. Kang,
D. Patnaik, J. F. Cortes, Prof. J. A. Rogers
University of Illinois at Urbana-Champaign
Frederick Seitz Materials Research Laboratory
104 S. Goodwin Ave
Urbana, IL 61801, USA
E-mail: jrogers@illinois.edu



Dr. X. Huang
Missouri University of Science and Technology
Mechanical and Aerospace Engineering
400 West 13th Street, Rolla, MO 65409, USA

DOI: 10.1002/adma.201403164

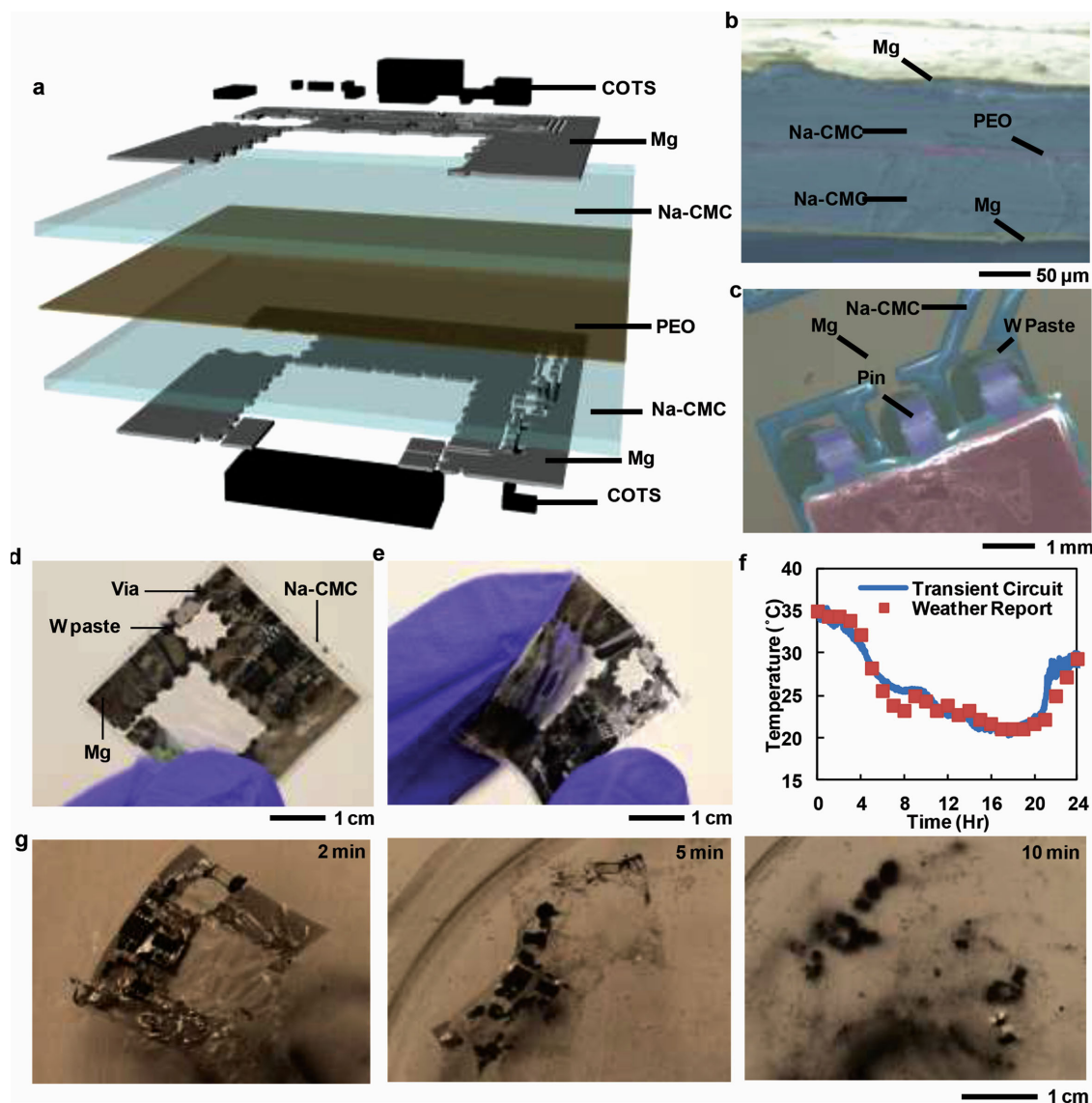


Figure 1. Representative transient PCB device. (a) Schematic exploded view illustration of stacked layers of water dissolvable polymer films, transient metal patterns, and commercial off-the-shelf (COTS) components. (b) Colorized SEM cross sectional image. (c) Colorized SEM image of a COTS component mounted using W paste. Pictures of a representative completed system in (d) flat and (e) bent geometries. (f) Environmental temperature measured and wirelessly transmitted using this device, with comparisons to data from a local weather report. (g). Dissolution of the device at three time points after immersion in water.

signal remains unchanged at -15 dBm throughout this range (Figure S2e). As the distance between the receiving antenna and the circuit increases from 0.7 to 4.2 m (Figure S2f), the measurement system (Figure S2a) records a power loss from -6.4 to -20.5 dBm. Benchtop systems can provide ultrasensitive signal detection (-160 dBm) (Figure S2a and S2b). Portable spectrum analyzers offer a compact alternative (Figure S2c). The results in Figure 1f show favorable comparison between the temperature measured by such a device and that from a local weather report, over a period of 24 hours (Figure 1f). The entire system disintegrates completely upon immersion in water for 10 mins (Figure 1g), leaving only the COTS chips and the transient metals, the latter of which react to yield soluble hydroxides on timescales of hours to days.^[20] The materials

in these PCB systems are biocompatible, although excessive amounts and concentrations can cause adverse effects.^[21] Controlled dissolution rates and protection from ambient water and water vapor can be achieved through the use of transient encapsulation layers and packaging materials. Candidates include previously studied inorganic materials such as MgO ,^[15] SiO_2 , Si_3N_4 ^[16] each of which has a comparatively slow dissolution rate.^[22] Bioresorbable polymers whose crystallinity, chemistry and/or molecular weight can be tuned to offer slow dissolution rates and low water permeability can also be considered.

Both Na-CMC and PEO are water soluble^[23,24] and biocompatible^[25,26]; each has been used in food, pharmaceuticals, and cosmetics as stabilizers for emulsions^[27,28] and thickeners.^[29,30] As cast, the Na-CMC films have a surface roughness of

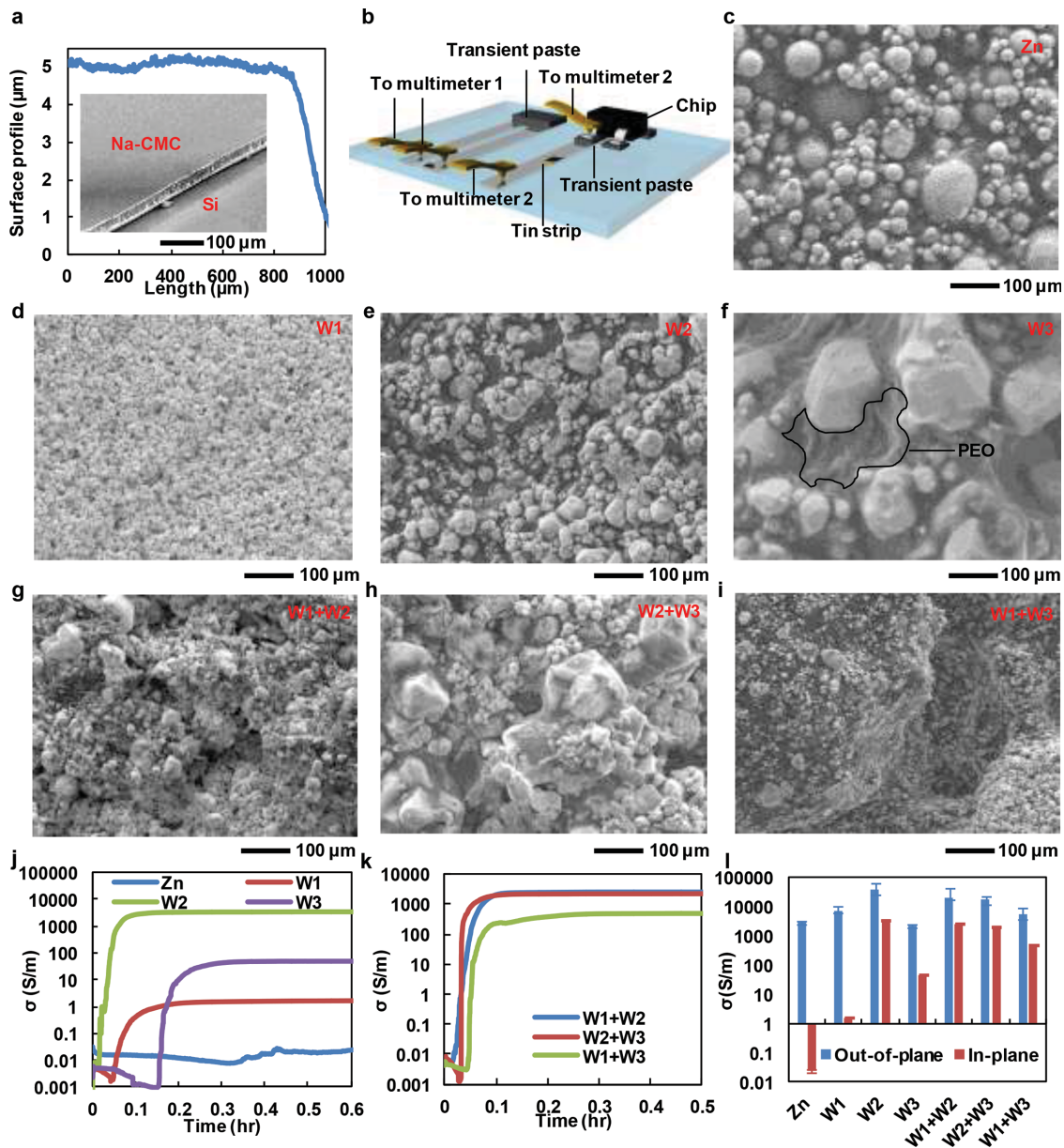


Figure 2. Materials for constructing transient PCB devices. (a) SEM image of a Na-CMC film on a silicon wafer. The smooth surface is important for defining continuous metal traces by physical vapor deposition. (b) Schematic exploded view illustration of the test structure used to measure the in- and out-of-plane conductivity of transient metal pastes. SEM images of materials for (c) Zn pastes and for W pastes based on six kinds of W particles: (d) W1 (0.6–1 μm), (e) W2 (4–6 μm), (f) W3 (12 μm), (g) W1+W2, (h) W2+W3, and (i) W1+W3. Time dependent variation in conductivity for pastes containing (j) uniform sizes of metal particles and (k) mixtures of different particle sizes. (l) Comparison of the out-of-plane and in-plane conductivity for all seven transient pastes.

~8–9 nm, evaluated by profilometry (Figure 2a). Transient pastes use microparticles of Zn (average diameters <10 nm; Figure 2c) or W (average diameters of 0.6–1 μm (W1), 4–6 μm (W2), 12 μm (W3), or mixtures of any two kinds of W particles at 1:2 weight ratio; Figure 2d–i) in PEO binders, to yield formulations that are compatible with screen printing. Three electroplated strips of tin (5 mm \times 20 mm each) spaced by 0.8 mm on a glass slide provide contacts for evaluating the electrical properties of these pastes (Figure 2b). Two of the strips enable measurement of the in-plane conductivity of a fixed volume of paste (~0.408 mm³) applied by screen printing. Measurements of the out-of-plane conductivity

use contacts between the third strips, on one side, and, on the other, the pins of COTS chips bonded on top via an applied layer of paste. All examined pastes show out-of-plane conductivities between 2000 and 40 000 S/m (Figure 2j) when cured for 10–20 min at room temperature. The in-plane conductivities vary significantly depending on formulation and curing time. The cured Zn paste has a value of 0.024 S/m (Figure 2l), likely limited by surface oxidation on the Zn particles and spherical shapes that result in point contacts (Figure 2c). The W2 paste has a conductivity (3500 S/m) higher than that of W1 (1.6 S/m) and W3 (47 S/m). All W pastes exhibit conductivities that increase during the

curing process (Figure 2j), with terminal values that are stable over longer times (Figure S3a). The conductivities, likely due to tunneling between adjacent particles,^[31,32] are comparable to those of commercial silver epoxies (5000 S/m).^[33,34]

The high conductivity of the W2 paste may arise, at least partly, from the polyhedral shapes of the W2 particles and the associated increased probabilities for physical contact over large areas (Figure 2e) between particles. The low conductivities of W1 and W3 paste can be attributed to other factors. The submicron sizes of the W1 particles can increase the physical contact between particles (Figure 2d), but with a high contact resistance.^[35] The comparatively large particles in the W3 paste result in a large porosity (Figure 2f), increased separation between particles and, thus, reduced chances for physical contacts. By mixing W particles at weight ratios (w.t.) of 1 (small particle sizes) to 2 (large particle size), all cases (W1+W2, W2+W3, W1+W3) show improved conductivities (2600, 2200, and 500 S/m, respectively), as might be expected based on considerations for pastes with W1 and W3 fillers (Figure 2g to 2i). Nevertheless, all mixed pastes still show lower conductivities than that of W2 only (Figure 2k). The W2 case also exhibits good mechanical bendability, as determined by coating the paste (~40 μm) on a strip of Na-CMC (~50 μm)

and conducting repeated bending tests with an automatic stage (Figure 3a and S6). In these tests, Na-CMC strips with conductive traces printed on their top surfaces are mechanically clamped at their ends, which present terminals for connection to a multimeter. For the radii of curvature examined here (3.5 mm), bending induces surface strains of ~1.3%. The observed changes in conductivity reversibly follow the bending, with no persistent change for over 1000 cycles.

Additional experiments reveal the dependence of the conductivity of the W2 paste on the weight of each component. A base solution of 1.5 g PEO and 10 g methanol mixed with W2 at weights between 20 g and 60 g (Figure 3b to 3f) shows that the in-plane conductivity achieves a maximum value of 4600 S/m at a filler weight of 40 g (Figure 3g and Figure S3b). A similar trend occurs with W3 fillers, although the conductivity is much lower (a maximum value at 100 S/m) compared to that of W2 (Figure 3g and Figure S3c). Investigations based on varying the weight of methanol (Figure 3h) and PEO (Figure 3i) with a fixed filler weight (40 g) indicate decreases in conductivity (from 4400 to 3500 S/m) with increases in methanol content (from 10 to 15g) and opposite trends (from 4400 to 5200 S/m) for increases in PEO (from 1.5 to 2.5g). The results suggest that

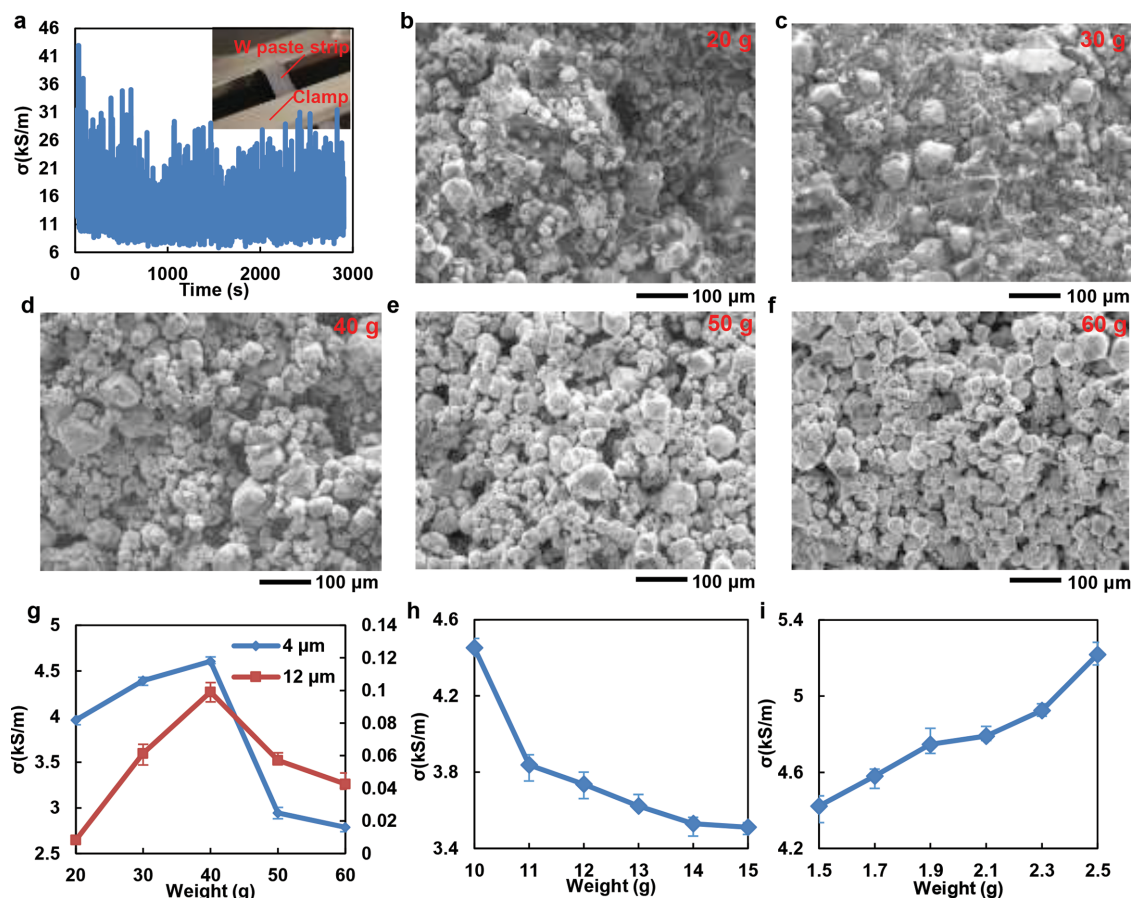


Figure 3. Parametric studies of the conductivities of W pastes. (a) Conductivity measured at two terminals of a conductive trace of W paste screen-printed on a Na-CMC strip as a function of cycles of bending (1000 times). SEM images of W paste with (b) 20 g, (c) 30g, (d) 40g, (e) 50 g, and (f) 60 g filler weight. (g) Comparison of conductivities of pastes with W2 and W3 fillers at different weight with a binder solution of 1.5 g PEO and 10 g methanol. (h) Conductivity of W paste with 40 g W2, 1.5 g PEO, as a function of the weight of methanol. (i) Conductivity of W paste with 40 g W2, 10 g methanol, as a function of the weight of PEO.

all three constituent parts affect the conductivity of the W paste, due to their combined roles in determining the paths for charge transport, shrinkage in physical dimensions due to curing, and ionic conduction associated with the binders.

Increases in efficiency of tunneling transport and physical contact area explain the increases in conductivity for pastes with W2 and W3 fillers at weights of 20 to 40 g^[36] (Figure 3b to 3d). However, further increases of filler weight lead to reduced volume fractions of the PEO and methanol, which result in diminished dimensional shrinkage and reduced binder coverage (Figure 3e and 3f), likely causing a decrease in the conductivity with addition of W particles. For experiments with increasing methanol levels (from 10 to 15 g), the reduced volume ratio of W in the paste (from 9.8% to 7.6%) likely overcomes the conductivity enhancement caused by out-of-plane shrinkage of the paste after curing. The increases in conductivity with weight of PEO (Figure 3i) may be explained by increases in the coverage of W particles with PEO and its ionic conductivity. The methanol can react with the W and surface oxide^[37,38] to form solid electrolytes with PEO,^[39–41] in a way that may facilitate ionic conduction between W particles. Impedance measurements of cured pastes with various PEO

content (from 1.5 to 2.5g) using an impedance analyzer (from 1 MHz to 1.8 GHz) (Figure S4a and S4b) and a RLC meter (from 20 Hz to 1 MHz) (Figure S4c and S4d) confirm that increasing the PEO contents reduces the impedance at low frequency (20 Hz to 300 MHz). Resonance peaks occur at frequencies near 500 MHz in all cases, with largest magnitude in W paste with 2.5 g of PEO. These observations suggest significant ionic polarization effects, increasing with PEO contents. The difference in the impedance of the W paste gradually diminishes at higher frequency (680 MHz to 1.8 GHz) due to the reduced effect of ionic conduction.

Screen printing methods similar to those used in manufacturing of conventional PCBs are useful for fabricating transient analogs. As examples, screen-printed transient conductive pastes on Na-CMC substrates can yield circuits for wireless power harvesting and near field communication (NFC) devices. The harvester consists of a two-turn meander loop antenna with a line width of 1.5 mm and an overall size of 50×50 mm². The inner loop of consists of a straight line coil with a length of 33 mm on each edge; the other loop involves meander structures formed by four evenly distributed teeth on individual edges (Detailed geometry in Figure 4a). A load circuit formed

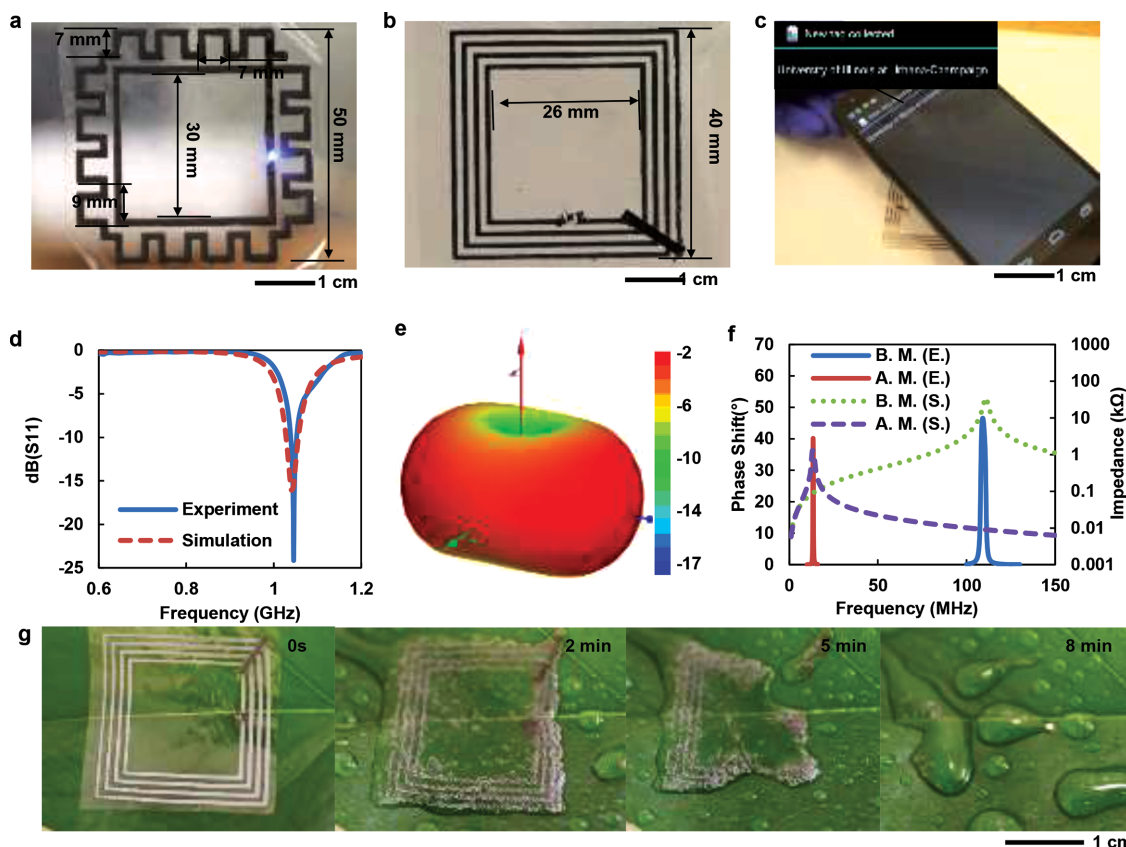


Figure 4. Printed transient RF antenna structures and PCB devices that incorporate them. (a) A transient RF power harvesting circuit with a meander loop antenna formed using a screen-printed W paste. The blue LED attached to the antenna demonstrates wireless power harvesting with an half-wave rectification circuit. (b) A transient NFC circuit with an inductive coupling coil. (c) Image showing readout of the NCF circuit using a cellphone. (d) Comparison of S11 as a function of frequency for a meander antenna obtained through measurement with a network analyzer and simulation using a commercial software package (Ansys HFSS). (e) Far-field radiation pattern of the meander loop antenna obtained using HFSS. (f) Frequency dependence of the phase shift and impedance of an NFC coil before (B.M.) and after (A.M.) capacitance matching obtained through inductive coupling method (E.) and simulation using HFSS (S.). (g) Dissolution of an NFC coil on a leaf under a gentle spray of water.

by a half-wave rectifier and an LED connects to the antenna for demonstrations of power harvesting from an external RF source. The LED can operate at a distance of 1 m from a transmission antenna that provides a power output of 20 W at 1.03 GHz (Figure 4a). An infrared image (Figure S5) indicates negligible changes in temperature in the vicinity of the antenna (highlighted by box 1) and increases of 7 °C near the load circuit (box 2). Such results are consistent with power dissipation primarily in the load, as expected based on the design. The S11 parameters of the meander loop antenna obtained using a network analyzer reveal a working frequency of ~1.04 GHz, consistent with simulated results (Ansys HFSS, Canonsburg, PA, USA). The far field radiation pattern obtained by HFSS has an expected donut shape with a maximum gain of ~ -2 dB in the plane of the antenna.

Figure 4b shows a four-turn NFC coil with a line-width of 1 mm and an overall dimension of 40 mm × 40 mm. The edge of the inner turn of the coil is 26 mm, and the spacing between individual turns is 1 mm. The coil exhibits a resonance frequency at 109 MHz as determined using an impedance analyzer, consistent with HFSS (Figure 4f). By adding a 130 pF capacitor and a NFC chip (Mifare Classic, NXP Semiconductors, Eindhoven, Netherlands) with an input capacitance of 17 pF, the resonance frequency of the coil can be tuned to 13.5 MHz, thereby matching the frequency of the NFC. Information can be retrieved with any NFC enabled Android smartphone (Figure 4c). The entire system, except for the COTS chips, dissolves under a spray of water within a few minutes (Figure 4g and Movie S1).

In summary, the results reported here establish a set of materials and methods for transient PCBs with performance comparable to that of conventional devices, but with the capability for dissolving into benign end products upon immersion in water. The transient printable conductive pastes are useful not only in this context but also separately for antennas, resonant coils and other components. Further improvements in the conductivities might be possible by increasing the shape anisotropy of the metal particles to reduce the percolation thresholds^[42] or by exploiting low temperature pulsed ultraviolet sintering techniques to facilitate physical contacts between particles^[43–45]. The designs and materials presented here are also applicable to rigid transient PCB circuits. Here, stacked layers of PEO and Na-CMC can offer improved rigidity, simply by increasing the thickness, thereby leading to a rigid transient PCB substrate. In addition, bioabsorbable materials such as poly(lactide) (PLA), poly(glycolide) (PGA), and poly (Lactide-co-Glycolide) (PLGA)^[46] each of which has been used as rigid fixture for implantable applications in orthopaedics^[47,48] and drug release systems,^[49,50] can serve as alternatives.

Experimental Section

The Na-CMC polymer solution is formed by dissolving Na-CMC particles ((Sigma-Aldrich Co., St. Louis, MO, USA) with a molecular weight of 250 000 in water at 2 wt% with constant agitation at 600 rpm for over 2 hours. Passing the resulting solution through a Nylon filter (PELCO Precision Woven Mesh, 300 mesh) and then a syringe filter (Millex-HV 0.45 µm, EMD Millipore, Billerica, MA, USA) removes undissolved particulates. PEO (polyox N-80, Dow Chemical Co., Charleston, IL, USA)

is mixed with methanol to 20 wt% at 80 °C with constant agitation at 120 rpm for 1 hour. The resulting solution is then allowed to stand at 80 °C for 2 hours to yield a PEO anhydrous solution.

Zn (Sigma-Aldrich Co., St. Louis, MO, USA) and W (Inframart Advanced Materials, LLC, Manchester, CT, USA) pastes are prepared using metal microparticles with average diameters between 4 and 10 µm. Preparation begins with addition of microparticles to methanol at 80 wt% in a glove box filled with Argon. The resulting mixture is then combined with PEO particles at 15 wt% with respect to the methanol, followed by 120 rpm agitation for 1 hour at 80 °C and standing at the same temperature for an additional hour.

The fabrication of the transient PCB circuit starts with casting 9 mL of 2% Na-CMC solution onto a 3 inch silicon wafer, followed by curing at 50 °C for 2 hours. A polyimide film (thickness 75 µm) with laser cut openings in the desired circuit geometry attaches to the Na-CMC film to serve as a shadow mask for electron beam deposition of 2 µm of Mg. The resulting film can be manually delaminated from the wafer. Two films fabricated in this manner, each with a different circuit pattern, are then aligned and bonded together using a solution of PEO in methanol.

The circuit for wireless temperature sensing (Figure S7a) incorporates two stacked layers bound together with PEO (Figure 1a). The bottom circuit provides signal conditioning and includes a receiving antenna (868 MHz; ILA. 02, Taoglas Limited, San Diego, CA, USA) and a voltage quadrupler (Figure S7b). This circuit converts RF energy received by the antenna into DC power with an amplitude four times larger than the voltage amplitude available at the antenna. The top circuit, which connects to the bottom circuit through vias filled with W paste, contains a voltage regulator (TC1014, Microchip Technology Inc., Chandler, Arizona, USA), a temperature sensor (LM20, Texas Instruments Inc., Dallas, Texas, USA), and a voltage controlled oscillator (MAX2750, Maxim Integrated, San Jose, CA, USA) (Figure S7c). The voltage control oscillator sends a continuous frequency-modulated RF signal determined by V_{tuner} , the voltage output from the temperature sensor, to an external signal analyzer through a 2.3–2.5 GHz antenna (WLA. 01, Taoglas Limited, San Diego, CA, USA).

Similar procedures enable fabrication of the meander loop antenna and the NFC coil (Figure S8). Taking the loop antenna as example, a pattern of Mg (1 µm in thickness) is formed on a Na-CMC film on a silicon wafer by electron beam evaporation. Next, a W paste (100 µm in thickness) is printed on top of this pattern using a 230 mesh nylon screen. A similarly patterned interconnecting bridge of W paste connects the inner terminal with the outer terminal of the antenna. The gap between the bridge and the antenna is filled with PEO solution, to form a dielectric layer (20 µm in thickness) after curing. Peeling the resulting film from the Si wafer allows mounting of electrical components with W paste to complete the fabrication.

The experimental setup for the wireless temperature sensing circuit appears in Figure S2. The system includes a HP 8648A RF signal generator (Agilent Technologies, Santa Clara, CA, USA) that provides a -10 dBm RF signal at 868 MHz to an RF power amplifier (Module 1119, Empower RF Systems, Inglewood, CA, USA) with a 20 W output. This power is transmitted through a wideband antenna (Modal 204411, Wilson Electronics, St. George, UT, USA) with a working frequency from 700 MHz to 2.7 GHz and a gain of 10.5 dBi. To receive the RF signal from the wireless temperature sensing circuit, an antenna (PA2419, ARC Wireless, Deland, FL, USA) with a working frequency from 2.3 to 2.5 GHz is used. The received signal is amplified by a RF amplifier (MGA-3-27, RF Bay, Inc., Rockville, MD, USA) and then displayed and recorded using a N9000A spectrum analyzer (Agilent Technologies, Santa Clara, CA, USA). Wireless powering of the LED with a meander loop antenna is demonstrated using the same experimental setup. The scattering parameters of the meander loop antenna are measured using an E5062A network analyzer (Agilent Technologies, Santa Clara, CA, USA) with home-made two point probes in contact with the antenna output ports (Figure S1b). The resonance frequency of the NFC RFID coil is measured using a setup introduced previously.^[51,52] Briefly, the transient coil is evaluated using a HP 4291A impedance analyzer (Agilent Technologies, Santa Clara, CA, USA) that connects to a one-turn hand-wound copper

primary coil placed 2 mm away from the transient coil. The impedance phase of the primary coil measured by the analyzer exhibits a phase peak/dip at a frequency close to the resonance frequency of the transient coil.

Supporting Information

Supporting Information is available from the Wiley Online Library or from the author.

Acknowledgements

The facilities for characterization and analysis were provided by the Material Research Laboratory and Center for Microanalysis of Materials at the University of Illinois at Urbana-Champaign, both of which are supported by the U.S. Department of Energy. The research was funded by an NSF INSPIRE grant.

Received: July 15, 2014

Revised: August 21, 2014

Published online: September 22, 2014

- [1] F. T. Wallenberger, P. A. Bingham, A. Longobardo, in *Fiberglass and Glass Technology*, Springer US, **2010**, 175.
- [2] B. H. Robinson, *Sci. Total Environ.* **2009**, *408*, 183.
- [3] L. Luther, *Managing Electronic Waste: Issues with Exporting E-Waste*, DIANE Publishing Company, **2010**.
- [4] A. Leung, Z. W. Cai, M. H. Wong, *J. Mater. Cycles Waste Manage.* **2006**, *8*, 21.
- [5] R. Widmer, H. Oswald-Krapf, D. Sinha-Khetriwal, M. Schnellmann, H. Böni, *Environ. Impact Assess. Rev.* **2005**, *25*, 436.
- [6] K. Grant, F. C. Goldizen, P. D. Sly, M.-N. Brune, M. Neira, M. van den Berg, R. E. Norman, *Lancet Glob. Health* **2013**, *1*, e350.
- [7] A. Terazono, S. Murakami, N. Abe, B. Inanc, Y. Moriguchi, S.-i. Sakai, M. Kojima, A. Yoshida, J. Li, J. Yang, M. H. Wong, A. Jain, I.-S. Kim, G. L. Peralta, C.-C. Lin, T. Mungcharoen, E. Williams, *J. Mater. Cycles Waste Manage.* **2006**, *8*, 1.
- [8] D. H. P. Kang, M. Chen, O. A. Ogunseitan, *Environ. Sci. Technol.* **2013**, *47*, 5495.
- [9] D. Xiang, P. Mou, J. Wang, G. Duan, H. Zhang, *Int. J. Adv. Manuf. Technol.* **2007**, *34*, 1030.
- [10] J. Li, H. Lu, J. Guo, Z. Xu, Y. Zhou, *Environ. Sci. Technol.* **2007**, *41*, 1995.
- [11] H.-Y. Kang, J. M. Schoenung, *Resour. Conserv. Recy.* **2005**, *45*, 368.
- [12] W. J. Deng, J. S. Zheng, X. H. Bi, J. M. Fu, M. H. Wong, *Environ. Int.* **2007**, *33*, 1063.
- [13] X. Xu, H. Yang, A. Chen, Y. Zhou, K. Wu, J. Liu, Y. Zhang, X. Huo, *Reprod. Toxicol.* **2012**, *33*, 94.
- [14] K. Huang, J. Guo, Z. Xu, *J. Hazard. Mater.* **2009**, *164*, 399.
- [15] S.-W. Hwang, H. Tao, D.-H. Kim, H. Cheng, J.-K. Song, E. Rill, M. A. Brenckle, B. Panilaitis, S. M. Won, Y.-S. Kim, Y. M. Song, K. J. Yu, A. Ameen, R. Li, Y. Su, M. Yang, D. L. Kaplan, M. R. Zakin, M. J. Slepian, Y. Huang, F. G. Omenetto, J. A. Rogers, *Science* **2012**, *337*, 1640.
- [16] S.-W. Hwang, D.-H. Kim, H. Tao, T.-i. Kim, S. Kim, K. J. Yu, B. Panilaitis, J.-W. Jeong, J.-K. Song, F. G. Omenetto, J. A. Rogers, *Adv. Funct. Mater.* **2013**, *23*, 4087.
- [17] C. Dagdeviren, S.-W. Hwang, Y. Su, S. Kim, H. Cheng, O. Gur, R. Haney, F. G. Omenetto, Y. Huang, J. A. Rogers, *Small* **2013**, *9*, 3398.
- [18] L. Yin, X. Huang, H. Xu, Y. Zhang, J. Lam, J. Cheng, J. A. Rogers, *Adv. Mater.* **2014**, *26*, 3879.
- [19] S.-W. Hwang, X. Huang, J.-H. Seo, J.-K. Song, S. Kim, S. Hage-Ali, H.-J. Chung, H. Tao, F. G. Omenetto, Z. Ma, J. A. Rogers, *Adv. Mater.* **2013**, *25*, 3526.
- [20] L. Yin, H. Cheng, S. Mao, R. Haasch, Y. Liu, X. Xie, S.-W. Hwang, H. Jain, S.-K. Kang, Y. Su, R. Li, Y. Huang, J. A. Rogers, *Adv. Funct. Mater.* **2014**, *24*, 644.
- [21] G. J. Fosmire, *Am. J. Clin. Nutr.* **1990**, *51*, 225.
- [22] S.-K. Kang, S.-W. Hwang, H. Cheng, S. Yu, B. H. Kim, J.-H. Kim, Y. Huang, J. A. Rogers, *Adv. Funct. Mater.* **2014**, *24*, 4427.
- [23] H. A. Shelanski, A. M. Clark, *J. Food Sci.* **1948**, *13*, 29.
- [24] J. Israelachvili, *Proc. Natl. Acad. Sci. U.S.A.* **1997**, *94*, 8378.
- [25] A. Hebeish, M. Hashem, M. M. A. El-Hady, S. Sharaf, *Carbohydr. Polym.* **2013**, *92*, 407.
- [26] C. Weber, R. Hoogenboom, U. S. Schubert, *Prog. Polym. Sci.* **2012**, *37*, 686.
- [27] M. Adeyeye, A. Jain, M. M. Ghorab, W. Reilly, *AAPS PharmSciTech* **2002**, *3*, 16.
- [28] N. Diftis, V. Kiosseoglou, *Food Chem.* **2003**, *81*, 1.
- [29] K. Pal, A. K. Banthia, D. K. Majumdar, *Biomed. Mater.* **2006**, *1*, 85.
- [30] S. Bayarri, L. González-Tomás, E. Costell, *Food Hydrocoll.* **2009**, *23*, 441.
- [31] S. Kirkpatrick, *Rev. Mod. Phys.* **1973**, *45*, 574.
- [32] S. M. Aharoni, *J. Appl. Phys.* **1972**, *43*, 2463.
- [33] MG Chemicals, 8331 Silver Conductive Epoxy Adhesive, <http://www.mgchemicals.com/products/adhesives/electrically-conductive/silver-conductive-epoxy-8331/>.
- [34] Structure Probe, Inc., SPI COnductive Silver Epoxy, http://www.2spi.com/catalog/spec_prep/inform.html.
- [35] H. H. Lee, K. S. Chou, Z. W. Shih, *Int. J. Adhes. Adhes.* **2005**, *25*, 437.
- [36] E. Sancaktar, L. Bai, *Polymers* **2011**, *3*, 427.
- [37] R. S. Mann, S. K. Jain, M. K. Dosi, *J. Appl. Chem. Biotechnol.* **1977**, *27*, 198.
- [38] K.-W. Park, K.-S. Ahn, Y.-C. Nah, J.-H. Choi, Y.-E. Sung, *J. Phys. Chem. B* **2003**, *107*, 4352.
- [39] W. Preechatiwong, J. M. Schultz, *Polymer* **1996**, *37*, 5109.
- [40] W. Wiecezorek, D. Raducha, A. Zalewska, J. R. Stevens, *J. Phys. Chem. B* **1998**, *102*, 8725.
- [41] X. Li, Y. Zhao, L. Cheng, M. Yan, X. Zheng, Z. Gao, Z. Jiang, *J. Solid State Electrochem.* **2005**, *9*, 609.
- [42] A. Aharony, D. Stauffer, *Introduction To Percolation Theory*, Taylor & Francis, **2003**.
- [43] R. Dharmadasa, I. M. Dharmadasa, T. Druffel, *Adv. Eng. Mater.* **2014**, n/a.
- [44] D. J. Lee, S. H. Park, S. Jang, H. S. Kim, J. H. Oh, Y. W. Song, *J. Micromech. Microeng.* **2011**, *21*, 125023.
- [45] H.-S. Kim, S. Dhage, D.-E. Shim, H. T. Hahn, *Appl. Phys. A* **2009**, *97*, 791.
- [46] J. C. Middleton, A. J. Tipton, *Biomaterials* **2000**, *21*, 2335.
- [47] C. Ambrose, T. Clanton, *Ann. Biomed. Eng.* **2004**, *32*, 171.
- [48] K. A. Athanasiou, C. M. Agrawal, F. A. Barber, S. S. Burkhart, *Arthroscopy* **1998**, *14*, 726.
- [49] H. K. Makadia, S. J. Siegel, *Polymers* **2011**, *3*, 1377.
- [50] H. A. Gad, M. A. El-Nabarawi, S. S. Abd El-Hady, *AAPS PharmSciTech* **2008**, *9*, 878.
- [51] X. Huang, Y. Liu, K. Chen, W.-J. Shin, C.-J. Lu, G.-W. Kong, D. Patnaik, S.-H. Lee, J. F. Cortes, J. A. Rogers, *Small* **2014**, *10*, 3083.
- [52] X. Huang, Y. Liu, H. Cheng, W.-J. Shin, J. A. Fan, Z. Liu, C.-J. Lu, G.-W. Kong, K. Chen, D. Patnaik, S.-H. Lee, S. Hage-Ali, Y. Huang, J. A. Rogers, *Adv. Funct. Mater.* **2014**, *24*, 3846.